Topographic control of wind-driven circulation in the northern Adriatic

V. Malačič,[1] B. Petelin,[1] and M. Vodopivec[1]

Received 19 March 2012; revised 16 May 2012; accepted 23 May 2012; published 30 June 2012.

[1] Two synoptic wind-driven situations of the circulation in the northern Adriatic were studied using the Princeton Ocean Model over the northern Adriatic Sea (NAPOM). In both situations the basin was driven by a relatively steady wind (>8 m/s) along and across the basin over three days. In the first situation (28–30 October 2008) the SSE southern jugo or scirocco wind blew along the basin, and in the second (19–21 March 2009), the ENE bora wind blew across the basin. Cyclonic turn was present in the first situation, while the cyclonic branch of a known double-gyre circulation north of the strip of wind minima was evident in the second. We show that during the jugo the model does not confirm quantitatively the simple topographic control of a wind-driven circulation, suitable for elongated basins, while qualitatively the model meets expectations, with downwind transport in shallow areas close to shorelines and upwind transport in places with greater depths. During the bora wind, however, the wind-driven circulation in the Gulf of Trieste is well explained by this topographic control (82% of the flux through the transect).

Citation: Malačič, V., B. Petelin, and M. Vodopivec (2012), Topographic control of wind-driven circulation in the northern Adriatic, *J. Geophys. Res.*, *117*, C06032, doi:10.1029/2012JC008063.

1. Introduction

[2] Numerical modeling of the circulation of the northern Adriatic has an extensive history. Partial reviews of efforts are available [*Poulain and Cushman-Roisin*, 2001; *Poulain et al.*, 2001] and one can hardly enumerate all the various modeling attempts, though we may reasonably assume that they seriously began in the 1970s with 1D models for the exploration of storm-surges and wind-driven currents/transport [*Accerboni et al.*, 1971; *Robinson et al.*, 1973], causing the flooding of the Venice lagoon. In this respect the role of the southern (SSE) jugo or scirocco wind is important, since it blows over the whole Adriatic Sea and is the second most frequent wind [*Jeromel et al.*, 2009].

[3] Modeling of the Adriatic Sea continued with a series of 2D (linear) model simulations, either of storm-surge currents under the southern wind with a constant depth [e.g., *Stravisi*, 1972], or simulations of transports for the Adriatic with a variable depth, driven by the jugo wind [*Stravisi*, 1973]. However, over the last decades modeling studies of wind-driven circulation during the jugo wind were less frequent than those simulating the circulation forced by the ENE bora wind. The inhomogeneity of the jugo wind, increasing toward the eastern coastline, leads to cyclonic vorticity [*Orlić et al.*, 1994].

[4] Modeling efforts continued with models of parts of the Adriatic, e.g., the northern Adriatic, during a (homogeneous) ENE bora wind [*Stravisi*, 1977], the most frequent wind [*Jeromel et al.*, 2009], or modeling a region along the Italian coastline in the mid-Adriatic [*Rizzoli and Bergamasco*, 1983] with a 3D (multilevel) model. The coastal area south of the Po River Delta is related to the situation in the northern Adriatic. It was found that the bottom torque dominates in the balance of forces in a vertically integrated alongshore flow when an alongshore density gradient (due to Po River outflow) is present. A complex, vertically integrated model, which resolved the equation of stream function [*Hendershott and Rizzoli*, 1976], in which time dependence enters through the equation of density, explored the importance of heat loss during the winter ENE bora wind. Another solid example of 3D modeling applies the method of eigenfunctions along the vertical [*Heaps*, 1972] for wind-driven circulation under the ENE bora over the northern Adriatic [*Kuzmić et al.*, 1985], where the controlling influence of a shallower topography along the western, Italian, coastline was revealed. The model with topography reproduced an intense coastal current, which was absent in a model with a flat bottom. The bottom topography meshes with the wind-curl in an adequate description of wind-driven circulation [*Orlić et al.*, 1986]. It was found that alongshore dynamics is well reproduced by a balance between wind stress and bottom stress, and that when wind stress torque is applied (from climatic estimates) the match with observations of currents at a platform ('Panon', bottom depth 28 m, November–December 1978) was better: The importance of wind stress vorticity during the ENE bora wind for a better (proper) reproduction of a current field in the form of a double gyre circulation, with currents that oppose the wind along its minima, was later pointed out in

[1]Marine Biology Station, National Institute of Biology, Piran, Slovenia.

Corresponding author: V. Malačič, Marine Biology Station, National Institute of Biology, Fornace 41, Piran 6330, Slovenia. (malacic@mbss.org)

0148-0227/12/2012JC008063

several studies [*Kuzmić et al.*, 2006; *Lee et al.*, 2005; *Martin et al.*, 2006; *Orlić et al.*, 1994; *Pullen et al.*, 2003; *Zore-Armanda and Gačić*, 1987]. The spread of the freshwater of the Po River outlet was also studied in relation to temperature and salinity as a response to the bora wind and the Po River outflow [*Jeffries and Lee*, 2007].

[5] A major obstacle to adequate simulation of wind-driven circulation is caused by the structure of the wind field, which is not well represented by atmospheric forecast models if their resolution is coarser than 10 km (e.g., the ECMWF), which has been clearly pointed out in studies [*Kuzmić et al.*, 2006; *Paklar et al.*, 2001]. In this sense the coupled ocean-atmosphere models (COAMPS) seem to lead in the right direction [*Kuzmić et al.*, 2006; *Martin et al.*, 2006; *Pullen et al.*, 2003].

[6] The mesoscale structures also evolve after a strong bora event winds down [*Cushman-Roisin and Korotenko*, 2007], at which time a geostrophic adjustment also takes place, especially after a bora in summer. Simulations during the winter bora reproduced the oblique current that drives the surface fresh water from the Po River outflow toward the Gulf of Trieste, for which the horizontal gradient of surface cooling along the axis of the northern Adriatic, with colder water along the northern, closed side of the northern Adriatic, seems to be responsible [*Cushman-Roisin and Korotenko*, 2007]. This finding is comparable to conclusions in an earlier study [*Hendershott and Rizzoli*, 1976], in which it was pointed out that during the bora the inflow of freshwater together with a strong horizontal density gradient set up by evaporation are a source for the winter dynamics and that the mass exchange with the southern Adriatic is then of secondary importance. The analysis of satellite images [*Bignami et al.*, 2007] revealed that during the bora turbid waters are exported offshore at the Po River Delta (Ancona headland) during the colder months when the daily Po River discharge surpasses 500 m^3/s (1000 m^3/s). During jugo wind events the offshore transport is not present, instead the shape of the WAC (western Adriatic current) front is locally modified.

[7] Recently [*Boldrin et al.*, 2009], a study focusing on changes in oceanographic conditions with bora pulses in a stratified sea also confirmed this finding (see *Boldrin et al.* [2009, Figure 6], who show a stronger decrease in surface temperature near the closed northern end of the Adriatic), but also pointed out the formation of a coastal current along this northern end. Moreover, in a situation when both bora jets were present, one that emerges from the Gulf of Trieste and the other from the Bay of Kvarner (26 September 2006, meteorological COAMPS model in *Boldrin et al.* [2009, Figure 3]), an intensification of the coastal current flowing along the Italian coast south of the Po River outlet was produced (case b in *Boldrin et al.* [2009, Figure 4]) using a ROMS model. It was also shown [*Boldrin et al.*, 2009] that concentrations of inorganic dissolved nutrients in the bottom water increased with the release of nutrients from the sediment and with the mineralization processes triggered by the resuspension of bottom layer sediment during bora events.

[8] From the time evolution of currents and sea-surface elevation in this work we will show that semidiurnal and diurnal tidal oscillations are present. These are just 'strong enough' to modulate currents, while they are insignificant from the point of view of the transport of a water mass over distances larger than a few km. The analysis of residual tides [*Cushman-Roisin et al.*, 2001; *Janeković and Kuzmić*, 2005; *Malačič and Viezzoli*, 2000] has shown that they are strong only around sharp promontories (e.g., the Po River outlet, the southern tip of the peninsula of Istria). Therefore, although tides have to be included for the sake of model credibility, they are not an issue in this paper, nor are the inertial currents that have also been studied in the northern Adriatic [*Krajcar and Orlić*, 1995; *Orlić*, 1987; *Orlić and Pasarić*, 2011]. They will be given proper attention in the Discussion section.

[9] This paper will explore/confirm the validity of a simple topographic control theory of wind-driven circulation with a numerical synoptic forecast model of circulation (northern Adriatic Princeton Ocean Model, NAPOM). It is organized as follows: measurements and the northern Adriatic POM model (NAPOM) are described in section 2, which covers applied methods. This embraces the surface and open boundary conditions of the model, points to a weak stratification of the studied examples and to the method of validation of model results with measurements from a coastal buoy. Section 3 presents the theory of a topographic control, section 4 covers results, while discussion and conclusions are in section 5.

2. Measurements and Model Set Up

[10] Currents and winds were measured using the coastal buoy Vida (www.buoy.mbss.org; The red dot on the red dashed line in Figure 1 marks the location). Wind measurements at a height 5 m above mean sea level were conducted using the 3D acoustic anemometer 'Wind Master Pro' of 'Gill's Instruments'. They were sent every 15 min with the microwave Ethernet link to the receiving station about 5 km away, where post-processing was performed. This began with checking the factory labels of data validity and continued with the transformation of the data from the anemometer, which is tilted and inclined, into the east, north and 'up' components. The inclinations were measured with synchronous compass-tilt measurements (every 0.1 s pitch, roll and azimuth). Post-processing was followed by quality control of these values, and by the calculation of 15 min and 30 min averages, together with the calculations of other statistics (gusts) in these intervals. Data were inserted into two databases, one for raw data and the other for post-processed data. Wind measurements were multiplied by a factor 1.094, according to the power law $U_{10} = U_h\,(10/h)^{0.13}$, where h = 5 m, U is the wind speed and the subscripts denote the height above sea level [*World Meteorological Organization*, 1983], to accommodate measurements at 5 m height to a height of 10 m, at which ALADIN/SI model results were obtained.

[11] Currents were measured with the 600 kHz standalone AWAC acoustic profiler of the 'Nortek AS' company, placed at the seafloor near the coastal buoy. AWAC was connected to the control unit on board the buoy with a 60 m cable. AWAC measured currents for 10 min at intervals of 30 min, therefore fresh data came to the land station with the Ethernet microwave link every 30 min, where it was inserted into a relational database.

[12] The model domain of the northern Adriatic Princeton Ocean Model (NAPOM) is presented in Figure 1. It embraces an almost square area with a typical length of over 130 km, a

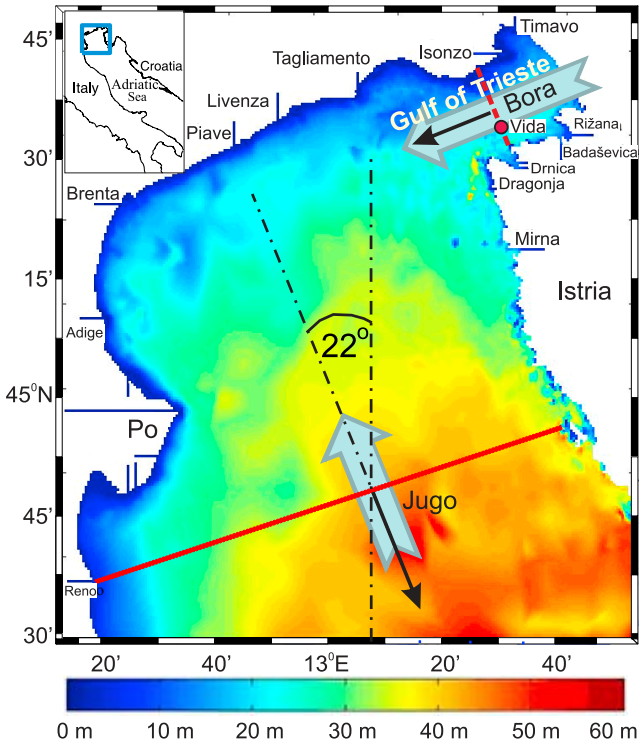

Figure 1. NAPOM model domain and its topography. The horizontal model resolution is around 600 m. The full red line represents the cross-section of the northern Adriatic, which is roughly orthogonal to the 'axis' of the northern Adriatic. The black arrows represent normal vectors to the transects and always point out of the 'interior': either out of the northern Adriatic (orthogonal to the full red line), or to the Gulf of Trieste (orthogonal to the dashed red line). The red dashed line that represents the cross-section in the Gulf of Trieste is orthogonal to the full red line. The ENE bora wind is parallel to the normal of the red dashed line. The red dot is position of buoy Vida. Rivers are represented as straight-line indentations in land. The values on the color bar at the bottom mean depths in meters.

wide southern open boundary (OB) line and a shorter eastward one, while on the northern, closed side, the Gulf of Trieste ('Gulf') in the northeastern corner is a wide open 'appendix' to the northern Adriatic. Depths on the southern side of the domain reach around 50 m, while typical depths inside the Gulf are around 15 m, with a maximum of 25 m in its central part. Figure 1 also shows the 'profile' lines (red full and red dashed lines) along which the vertical distribution of the flow will be explored during two synoptic wind-driven situations. The forecasted wind from the ALADIN/SI model will be compared with the measured wind on the coastal buoy 'Vida' (Figure 1, red dot). Closer to the goal of this work is, however, the comparison of modeled currents at that position with currents measured by the ADCP (AWAC) instrument at the seafloor.

[13] NAPOM with a horizontal resolution ~600 m (grid cell-dimensions: dx = 581 ± 4 m, dy = 604.0 ± 0.1 m) is one-way nested in the Adriatic Sea Forecasting System (ASFS) with ~2.5 km of horizontal resolution with 21 sigma levels, operated by INGV in Bologna (http://gnoo.bo.ingv.it/afs/). The predecessor of this model had a horizontal resolution of 5 km and 21 sigma levels [*Chiggiato and Oddo*, 2008; *Oddo et al.*, 2006]. NAPOM is initialized with forecasted values of temperature and salinity for the first next day, interpolated from the ASFS in NAPOM with 11 sigma levels (0, −0.06, −0.15, −0.26, −0.37, −0.48, −0.59, −0.70, −0.81, −0.91, −1.0).

2.1. Surface Boundary Conditions and Rivers

2.1.1. Momentum Flux

[14] The major forcing element in this study, wind stress, is imported into the model from the ALADIN/SI (http://meteo.arso.gov.si/met/en/app/webmet/) atmospheric forecast model [*Bénard et al.*, 2010], with a horizontal resolution of 9.5 km [*Pristov et al.*, 2011]. Two typical windy situations have been chosen. The situation with the second most frequent 'jugo' wind on 28–30 October 2008 and the situation with the most frequent ENE 'bora' wind on 19–21 March 2009. In both time intervals the wind was relatively strong and steady, blowing over three days (Figure 2). We see that the forecast of winds with the ALADIN/SI model nicely corresponds to winds measured at the coastal buoy Vida (see Figure 1 for the location). Since the horizontal resolution of the atmospheric model is low with respect to the resolution of the NAPOM model (600 m), the hourly value of the wind stress at mid-time of observing time intervals looks smooth over the 130 km of model domain (Figure 3). Still, the

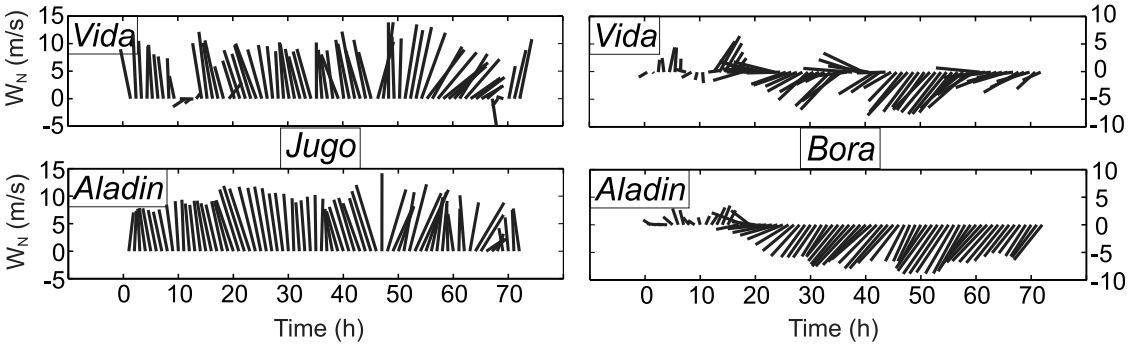

Figure 2. Stick plots of (top) wind speed measured on the buoy Vida and (bottom) forecasted hourly values of wind at 10 m height above sea level by the ALADIN/SI model (left) for the period 28–30 October 2008 during the 'jugo' or southern wind, and (right) for the period 19th–21st March 2009 during the bora (ENE) wind.

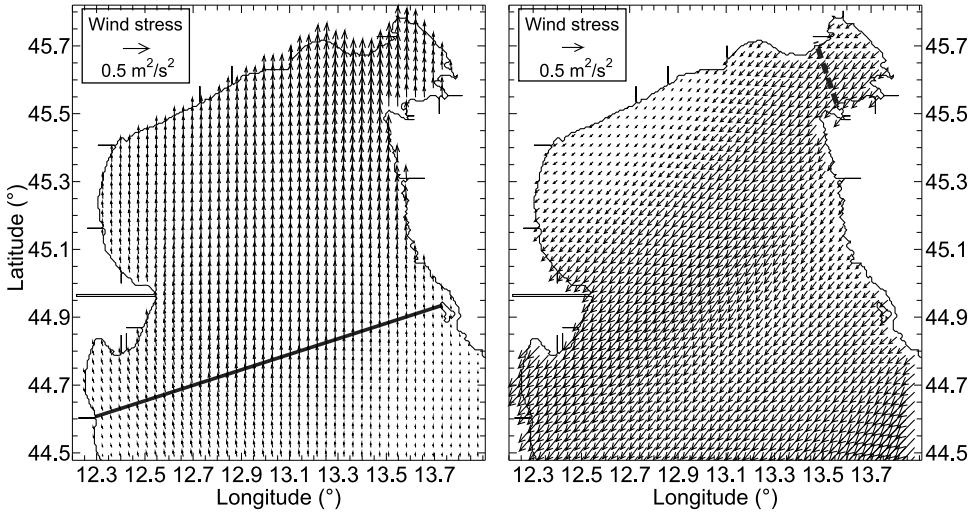

Figure 3. Horizontal distribution of the wind stress (left) during the southern jugo wind 36 h after 28th October 2008 and (right) during the ENE wind bora 36 h after 19th March 2009. Both are averages of hourly values of the ALADIN/SI forecast, interpolated on a NAPOM model grid. The full line represents the profile, along which the transport of water mass will be explored during the jugo wind, while the dashed line represents a profile along which a transport will be explored at the entrance to the Gulf of Trieste (Gulf) during the bora wind. Note that the jugo wind increases from the western coastline to the eastern, while the bora wind has minima along the line that connects points (50, 0) and (175, 75) and a line of maxima parallel to it, which emerges in the Gulf.

southern jugo wind (Figure 3, left) increases in speed from the westward to the eastward coastline of the model domain, with low winds in the southeastern model domain. The ENE bora wind (Figure 3, right) has a diagonal area of minima speeds along a diagonal line that connects points (12.7°E, 44.5°N) at the southern open boundary (OB) line and the point (13.6°E, 45.0°N) near the coastline of Istria. Northward is an area of local maxima of wind speeds, a bora jet that emerges from the Gulf of Trieste [*Dorman et al.*, 2007]. The second bora jet [*Dorman et al.*, 2007; *Lee et al.*, 2005], that emerges from the Bay of Kvarner southeastward of the model domain, is modestly reproduced with a triangular area south of the peninsula of Istria (longitude > 13.4°E, latitude < 44.8°N). The conservation of momentum was supposed across the sea-surface in passing the wind stress into the sea ($\rho_a\tau_a = \rho_w\tau_w$, where ρ_a and ρ_w are the densities of air and water at the sea-surface, and τ_a and τ_w are, respectively, stresses above and below the sea-surface).

[15] At the sea-surface the same boundary conditions for vertical heat and salinity fluxes are applied as in the climatic model of the Gulf of Trieste [*Malačič and Petelin*, 2009] and will not be repeated here.

[16] In the model, all forcing fields at the surface (heat flux, precipitation-evaporation and wind stress) were updated with hourly forecast values from the meteorological model ALADIN/SI [*Pristov et al.*, 2011]. However, linear interpolation in time for shorter time steps (e.g., 900 s for the internal mode in NAPOM) does not conserve hourly averages. For that reason *pseudo* average values [*Killworth*, 1996] were continuously applied.

2.1.2. River Discharges

[17] River estuaries of 14 rivers are aligned with the lines of a numerical grid of topography (sea-surface elevations) with a width that equals the horizontal dimension of the grid-cells (0.55–0.6 km). As found through numerical experiments [*Malačič and Petelin*, 2009], it is sufficient to impose about ten model cells 'upstream' from the river mouth along the estuary. Monthly values of river flow rates were imposed on the upstream-most cells in all sigma-levels with depth-averaged velocities in the downstream direction [*Marsaleix et al.*, 1998]. Salinity in the most upstream cells is zero, the sea-surface elevation and temperature were extrapolated from model cells around the mouths. The Po River dominates by far [*Raicich*, 1994]. Revisited monthly mean flow rates of rivers were applied along the eastern side of the model domain [*Malačič and Petelin*, 2009].

2.1.3. Boundary Conditions for Turbulent Kinetic Energy

[18] Turbulent kinetic energy becomes part of a set of surface boundary conditions. In the code of POM there is an option to additionally account for the effect of surface wave breaking on the increase of turbulent kinetic energy (TKE). In the Mellor-Yamada turbulence scheme [*Mellor and Yamada*, 1982] the TKE at the sea-surface ($z = 0$) is described in as:

$$q^2(0) = B_1^{2/3} u_*^2; \quad q^2 l(0) = 0, \tag{1}$$

where $B_1 = 16.6$, q^2 is twice the TKE, l the turbulence (master) length scale and u_* the friction velocity in the sea near the sea-surface. The first of the boundary conditions follows from the equation of TKE, in which it is supposed that the local time derivative of TKE and the vertical diffusion of TKE equal zero and that the dissipation of TKE is balanced by the shear production. Applying these conditions

in the balance of TKE [*Huang et al.*, 2011, equation 2a; *Mellor*, 2004, equation (1)] yields:

$$-\langle u'w'\rangle\left(\frac{\partial U}{\partial z}\right)-\varepsilon=0\Rightarrow u_*^2\frac{u_*}{l}-\frac{q^3}{B_1 l}=0 \qquad (2)$$

which results in the first equation in (1). In (2) it was supposed that the vertical flux of momentum $-\langle u'w'\rangle = u_*^2$ and that the shear ($\partial U/\partial z$) is approximated with u_*/l [*Mellor and Yamada*, 1982, equation 43a]. The second equation in (1) is simply added as a surface condition for $l(0)$, expressed as a condition for the composed model variable $q^2 l$ [*Mellor and Yamada*, 1982, equation 55]. In (2) the vertical eddy flux of TKE due to the vertical gradient of TKE is ignored, while in many studies [e.g., *Carniel et al.*, 2009] this term plays a role and it is parameterized at the sea-surface with u_*^3 – as is the shear production term in (2).

[19] However, when the contribution of surface-wave breaking to TKE is additionally considered, then (1) is replaced [*Huang et al.*, 2011] with:

$$q^2(0)=(K_1\alpha_{CB})^{2/3}u_*^2;\quad l(0)=\kappa z_w \qquad (3)$$

in which the surface roughness length scale at the sea-side is $z_w = \beta_{CB}\, u_*^2/g$, which is also introduced to the scale at the atmospheric side with another constant of proportionality [*Charnock*, 1955], while here $\beta_{CB} = 2\ 10^5$, $\alpha_{CB} = 100$ [*Craig and Banner*, 1994], g is gravity acceleration and $\kappa = 0.41$ the von Kárman constant. A review of the values of β_{CB} was also recently presented [*Carniel et al.*, 2009]. Some ambiguity is present in the value of K_1, which is either 15.8 [*Huang et al.*, 2011] or 16.6 (=B_1) [*Mellor and Blumberg*, 2004]. If one applies the wind speed W instead of u_*, it can be easily shown [*Stacey*, 1999] that the roughness length scale z_w ($\cong 0.2\ W^2/g$) is proportional, or close to the significant wave height H_s ($\cong 0.3\ W^2/g$) [*LeBlond and Mysak*, 1988].

[20] NAPOM with (3) has shown a quite small vertical variability of currents at the position of the coastal buoy Vida, much smaller than that manifested by measurements, especially during the bora wind, when it was observed that a strong downwind outflow is present near the surface, while only at depths greater than 3 m a compensating inflow exists [*Malačič and Petelin*, 2006], with currents almost the same down to the bottom. This sharp pith of currents at the surface was not reproduced with NAPOM when surface wave-breaking was considered in surface boundary conditions for q and l, as in (3), while a better reproduction of a vertical profile of currents was achieved with surface boundary conditions in (1). There is no doubt about the boundary condition for q^2 and $q^2 l$ at the seafloor: both are zero.

2.2. Open Boundary Conditions

[21] Along the open boundary of the NAPOM the radiation condition [*Mellor*, 2004] is applied that connects the 'barotropic' velocity V_a with the sea-surface elevation η. For the southern (longer) open boundary this means

$$V_a(i,j_0,t+\Delta t)=V_A(i,j_0,t)+V_{tide}(i,j_0,t)-\sqrt{g/H(i,j_0)}[\eta(i,j_0,t)-\eta_A(i,j_0,t)-\eta_{tide}(i,j_0,t)] \qquad (4)$$

in which j_0 (=2) is the value of the index in the 'y' (south-north) direction of the grid cells along the OB line, while $i = 1\ldots232$. V_A is the daily vertically integrated velocity, η_A the daily averaged elevation, both provided by ASFS.

[22] The radiation boundary condition (4) is one of the 'standard' possible conditions offered by POM [*Mellor*, 2004] and is the adapted 'Flather' boundary condition [*Flather*, 1976], widely applied [e.g., *Arnold*, 1987]. In the code the linear interpolation in time between daily averaged values V_A is applied at each barotropic time step ($\Delta t = 9$ s) with updating at each baroclinic time step of 900 s. The elevation η_A, also provided by the Adriatic model, is introduced in the same way. V_{tide} is the vertically averaged tidal velocity and η_{tide} the tidal elevation. Along the OB line values of V_{tide} and η_{tide} at each time step are computed from the analytical expression of the sum of seven tidal constituents. Amplitudes and phases were extracted along the OB line from a coarser tidal model [*Malačič and Petelin*, 2004] of the whole Adriatic Sea (modified AREG model, 5 km horizontal resolution), with the trigonometric least squares procedure [*Malačič and Viezzoli*, 2000; *Malačič et al.*, 2000] and values were interpolated to grid points of a higher resolution of NAPOM. The quantity η is the 'model' elevation calculated in a previous time step. η_A represents the baroclinic, 'slow' changes of the elevation, which holds for periods with steady wind after the wind setup. A similar boundary condition was applied for the eastern OB line south of the peninsula of Istria.

[23] The time series of η_{tide} along the OB lines for the two windy synoptic situations in Figure 4 (top) (black lines with black vertical bars) shows space variability (standard deviation, 'SD') of the elevation along the OB line. The SD results from the space variability of the amplitude and of the phase of each of seven major tidal constituents, among which four are semidiurnal, while three are diurnal [*Polli*, 1959]. The depth average velocity components U_n (black line with orange vertical bars), orthogonal to the OB lines (southern and eastern, see Figure 1), which resulted from the numerical model of tides of the whole Adriatic area, experience much larger SD at each hour with respect to their space average values in the period 28–30 October 2008 (Figure 4, top left), when tidal range is also much larger than that during 19–21 March 2009 (Figure 4, top right). One may also observe that within the first 17 h η_{tide} (and U_n) applied along the OB lines increase with time and are smaller than the predicted tides in the time >17 h because a linear time ramp with inertial time scale is applied at the beginning of the simulations to 'smooth' the gradients of quantities since the model was initialized with zero elevations and velocities. Resulting model elevations at the position of buoy Vida, affected by the wind field as well, are presented together with pressure measurements at the seafloor below buoy Vida for both windy situations (Figure 4, bottom). When for the situation during 28–30 October 2008 (southern jugo wind, Figure 4 (bottom left)) the annual average pressure value (=22.343 dbar) is subtracted from hourly measured pressure values (red line), the RMS difference between NAPOM and measured sea-surface elevation using the pressure sensor equals 0.138 m. However, when the three day average pressure (=22.497 dbar) is subtracted from the measured hourly pressure (blue line), one cannot distinguish whether the modeled elevation (black line) is closer to

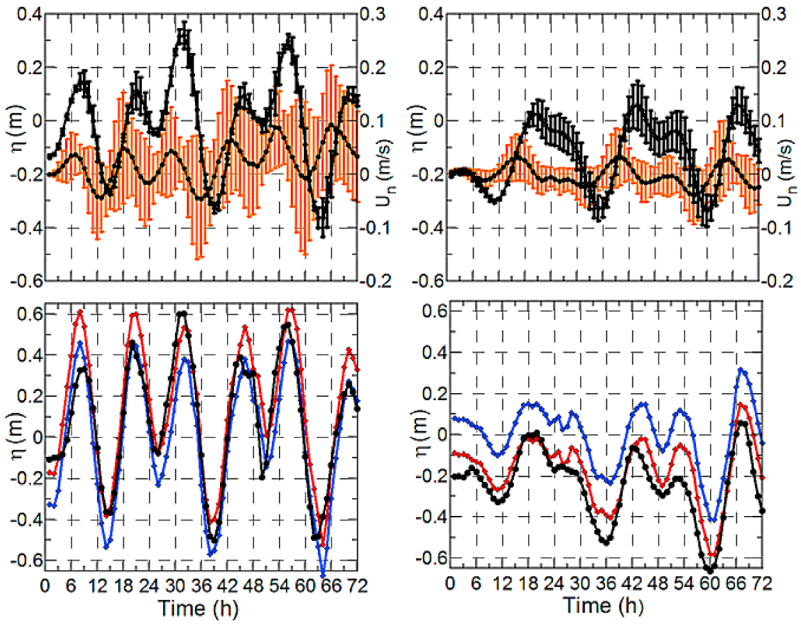

Figure 4. (top) Time series of sea-surface elevations η_{tide} (left axis) and depth-average velocities normal to the OB line U_n (right axis) due to tides along the OB lines (top left) in the period 28–30 October 2008 of the jugo southern wind and (top right) in the period 19–21 March 2009 of the ENE bora wind. Black lines with black bars represent space average value η at each hour, while the length of the vertical bar represents two standard deviations (SD) of space variation of η along the two OB lines. The same holds for U_n, except that the error bars are in orange. (bottom) Time series of η at the location of buoy Vida, among which are NAPOM elevations (black lines with dots), and measured pressure at the seafloor below Vida converted into heights, where either three day average pressure is subtracted from the measurements (blue lines with diamonds), or the average pressure value (=22.34 dbar) in year 2009 is subtracted from measurements (red lines with diamonds). (bottom left) The situation between 28–30 October 2008 and (bottom right) the situation between 19–21 March 2009.

the blue line, or to the red one, since it is evenly between them. During the ENE bora wind during 19–21 March 2009 (Figure 4, bottom right), however, the RMS difference between model elevation and that 'measured' with the pressure sensor equals only 0.096 m when the 2009 annual average pressure value is subtracted from the hourly values (red line). The RMS difference is 2.6 times larger (=0.252 m) when the three day average pressure (=22.174 dbar, blue line) is subtracted. This is manifested in a solid match between NAPOM elevations (black line) and the elevations in which the annual mean value is subtracted from the measured sea level (red line). The three-day mean sea level during the bora was lower than the average level in 2009 for 0.17 m – the bora wind-setup piles water up along the western Adriatic side (Venice) and decreases it along the eastern side (Trieste). During the southern jugo wind, however, the three day average sea level was higher for 0.15 m than the average sea level in 2009. The water mass was piled up at the northern closed side of the Adriatic. We may conclude at this point that, in a first approximation, the applied OB conditions related to periodic tides fairly well reproduce the sea level elevations at the position of Vida and that we may devote attention to wind-driven transport. Fluxes of heat and salinity along the OB lines have been approximated with the upstream advection scheme [*Mellor*, 2004]. Similarly, for the turbulent quantities q^2 (two times the turbulent kinetic energy) and q^2l (where l is the turbulence length scale), a common practice is adopted in which very small constant values are supposed for q^2 (=10^{-8} m^2/s^2) and q^2l (=10^{-8} m^3/s^2) instead of external values. All daily average values provided by the external forecast model ASFS that are introduced into this model, were first transformed into 'pseudo' values [*Killworth*, 1996] and thereafter interpolated linearly in time between them.

2.3. Mild Stratification

[24] Although we do not possess data which would depict relevant stratification over the whole model domain during the periods of the two observed synoptic situations of nearly steady winds, we may obtain an impression of it from CTD casts during those periods taken in the Gulf of Trieste (http://www.mbss.org/). In October 2008 and in March 2009 three CTD casts in the Gulf which comprise waters with depths greater than 20 m were taken. The density excess at 1 m depth in October 2008 (casts on 9 and 15 October) was 27.07 ± 0.19 kg/m^3, while at a depth of 15 m it was 27.22 ± 0.22 kg/m^3. This leads to the buoyancy frequency $N = (-g\Delta\rho/(\rho\Delta z))^{1/2}$ between 0 and 0.0198 s^{-1}, or the corresponding buoyancy period between 318 s and infinity. In March 2009 out of three CTD casts (on 17 and 24 March) only two were completed before the windy period (from 19 March onward). The density excess on 17 March 2009 at a depth of 1 m was 28.53 ± 0.19 kg/m^3, while at a depth of 15 m 29.08 ± 0.05 it was kg/m^3, which yields in

$N = (0.019 \pm 0.012)\ s^{-1}$, or a buoyancy period between 270–432 s. The buoyancy frequency of the initial fields of temperature and salinity, calculated from their horizontal averages at 1 m and at 15 m depths was around $(0.029 \pm 0.014)\ s^{-1}$ (period 213–223 s) on 28 October 2008, while on 19 March 2009 it was around $(0.0198 \pm 0.010)\ s^{-1}$ (period 307–328 s).

[25] We may conclude that for the situation in late October 2008 the initial stratification in the model was smaller than that measured on 9 and 15 October 2008 in the Gulf, which may not be that problematic since between 17 and 29 October additional surface cooling and forced wind-mixing homogenized the water column. For the situation on 19 March 2009 the stratification of the initial field (307–328 s) is covered by the interval of buoyancy period 270–432 s, measured only in the Gulf. In the bottom part of the water column, below 15 m, the stratification is, of course, even weaker. However, a slightly bold conclusion will here be proposed: in both synoptic situations, the one in late October 2008 and the other in mid-March 2009, a mild stratification did not play a dominant role in the processes of the transport of a water mass under wind speeds over 10 m/s and will be ignored for the sake of clarity, until the Discussion section.

2.4. Comparison of Model Results With Measurements

[26] A statistical analysis of model skill that is grounded here on a comparison of 'point' measurements at buoy Vida of winds with the forecast ALADIN/SI model results, as well as measurements of currents over the water column with the NAPOM results, will follow an established path [*Oke et al.*, 2002], which seems suitable for the available data. We shall briefly repeat the list of calculated quantities, by which a single model could be validated with measurements:

$$MB = (\bar{m} - \bar{o}), \quad SDE = (S_m - S_o),$$
$$CC = \frac{1}{S_m S_o N}\sum_{i=1}^{N}(m_i - \bar{m})(o_i - \bar{o}),$$
$$MSE = \frac{1}{N}\sum_{i=1}^{N}(m_i - o_i)^2 = MB^2 + SDE^2 + 2S_m S_o(1 - CC), \tag{5}$$

in which m_i and o_i are the i-th modeled and observed variable, $i = 1 \ldots N$, $N = 72$ when only three days of time series data are considered for each horizontal component (east and west) of winds. However, for currents, $N = 72*17 = 1224$, where the number 17 means the 17 mid-depths of acoustic cells along the vertical in the water column in which currents were measured and selected below the buoy Vida. Along the vertical there are 21 cells of a thickness of 1 m of measured currents with heights 2–22 m above the AWAC instrument, placed at a height ~0.5 m above the seafloor. $\bar{m}$ and $\bar{o}$ are respective mean values, while S_m and S_o are the respective standard deviations (in time) and CC is the cross-correlation coefficient between the modeled and observed values. MSE is the mean square error.

[27] We have removed measurements of the first cell next to the current-meter near the seafloor and the two top-most cells near the sea-surface due to the contamination of these measurements by the 'sidelobe' reflections of acoustic beams near the boundaries. The top most cell is also problematic because the range of the water column height (mean height 22.5 m) is of the order of a meter (Figure 4) and this cell might not be covered with water. There was an additional unknown problem with the eighth cell (9 m above the seafloor) in which we have observed spurious sharp peaks of current speed, of yet unknown origin. Therefore, out of 21 cells four were removed and measurements of currents in 17 cells of a thickness of 1 m in the water column were left for analysis. All hourly values at 17 depths within 72 h of observation were 'lumped' together in the skill analysis of NAPOM for each horizontal component of currents. In this case these are the components normal to the cross-section profile of the Gulf, as well as the tangential component parallel to the cross-section line.

[28] It is obvious that these measurements shed some light on the model forecasts only around the location of buoy Vida. This is located along the line of a profile in the Gulf of Trieste (Figure 1, red dot and a red dashed line) in which the simplified theory of a topographic control is explored during the ENE bora wind. It therefore cannot give us a solid impression about the model skill around the other, much longer profile of the cross-section (Figure 1, full red line) of the northern Adriatic.

3. Topographic Control of Water Mass Transport

[29] Let us suppose that the x-axis is along an elongated basin (a 'trunk', or a 'channel'), the y-axis across it, and from now on the water transport (U, V) is denoted with capital letters.

$$U = \int_{-H}^{\eta} u\,dz; \quad V = \int_{-H}^{\eta} v\,dz \tag{6}$$

$u(x, y, z)$ is the along basin component of velocity and $v(x, y, z)$ that of the cross-basin, $\eta(x, y)$ is the sea-surface elevation and $H(x, y)$ the depth of the seafloor. We will follow the textbook [*Csanady*, 1982] and simplify the equations of motion.

[30] Starting from the rest, we will gain an insight into a wind-driven transport if we express the transport with vertically integrated accelerations:

$$U = \int_{0}^{t} A\,dt; \quad V = \int_{0}^{t} B\,dt, \tag{7}$$

where we have supposed the initial transports to be zero.

[31] Let us suppose that the advective term is not important with respect to local acceleration, when a strong and steady wind 'suddenly' appears and that the loss of momentum due to bottom friction can also be ignored with respect to local acceleration. Under these stringent approximations the vertically integrated equation of motion looks like:

$$A - fV = -gH\frac{\partial \eta}{\partial x} + F; \quad B + fU = -gH\frac{\partial \eta}{\partial y}, \tag{8}$$

where f ($=10^{-4}$/s) is the Coriolis parameter and where we allow the wind stress $F(x, y, t)$ at the surface along the basin's axis to vary in space and time. We suppose that in

the basin the topography across the elongated basin controls the transport and that the along basin transport is much larger than the across-basin $U \gg V$, therefore also $A \gg B$.

[32] We also need to suppose that the Coriolis acceleration is small enough ($fU \leq B$), which leads from the cross-section balance of momentum in (8) to

$$\frac{\partial \eta}{\partial y} \cong 0. \tag{9}$$

[33] We will return to the treatment of the Coriolis acceleration in the Discussion section. The 'steady' (meaning the non-oscillating, as will be made clear in Discussion) along basin transport, when integrated across any basin cross section needs to be zero, or $L\langle U\rangle = 0$, where $\langle U\rangle$ is the cross-section average of the transport and $L(x)$ the width of the basin cross-section. Otherwise the flux through any cross-section would not conserve the volume of water mass at either side of it. Therefore, the integral of acceleration A across any cross-section of length L is also zero. From the along-channel balance of momentum in (8), integrated along the cross-section of length L, one obtains:

$$\frac{\partial \eta}{\partial x} = \frac{\langle F\rangle L}{gS}, \quad S(x) = \int_0^{L(x)} H(x,y)dy, \ \langle F\rangle(x,t) = \frac{1}{L}\int_0^{L(x)} F(x,y,t)dy. \tag{10}$$

[34] Where (9) was considered, $S(x)$ is obviously the cross-section area and $\langle F\rangle$ the wind stress average over the line of a cross-section. In (10) we have rectified the term that is proportional to $\int_0^L Vdy$ to zero, since it means the cross-section integral (average) of the transport component in a direction *along* the cross-section. This has to be zero unless the coastlines are not perpendicular to the cross-section. At this point we further assume that F does not vary across the transect, therefore $\langle F\rangle = F$. The along basin pressure gradient term from (10) in (8) results in the along basin transport velocity:

$$U(x,y,\tau) = \left[1 - \frac{H(x,y)L(x)}{S(x)}\right]\int_0^\tau Fdt \tag{11}$$

in which we considered that $f\int_0^\tau Vdt \ll U$. We may go a few steps further from (11) [*Csanady*, 1982] and first integrate the transport in (11) to get a mean transport in time and integrate also the mean transport in time across the cross-section and express the volume flux Φ_{tot} through the cross-section:

$$\Phi_{tot}(x) = \int_0^L \bar{U}(x,y)dy \propto \int_0^L \left[1 - \frac{H}{\langle H\rangle}\right]dy = 0, \tag{12}$$

where $\bar{U}$ is the transport averaged in time and where zero at the right-hand side of proportionality follows from the definition of the average cross-section depth, supposed already in (10), $\langle H\rangle(x) = S(x)/L(x)$ is the average depth across the profile. This is also in agreement with the initially supposed zero flux through any cross-section, which lead to (10). It means that the time average of the along basin transport, which is proportional to the argument inside the integral in (12), changes its sign at those places along the cross-section at a given x along the basing axis, for which $H(x, y) = \langle H\rangle(x)$. $\bar{U} > 0$ and is directed downwind F if $H < \langle H\rangle$, while $\bar{U} < 0$ and in the upwind direction when $H > \langle H\rangle$. In short: nearshores the time averaged transport $\bar{U}$ is downwind, while in the deeper (central) parts of a basin the transport is upwind. However, we also need to pay attention to horizontal gradients (e.g., $\partial U/\partial y$) which need to be smooth enough in order to ignore the advection terms with respect to local accelerations and that also $A \gg fV$, where f is the Coriolis parameter. The wind stress should not vary across the basin's cross-section.

[35] The deviation of Φ_{tot} from zero also represents one validation of (12), if we consider NAPOM values of $\bar{U}$ as references. This is a first validation of a simplified theory of topographic control with NAPOM. We will see that the deviation ε of Φ_{tot} from zero, relative to the average of absolute values of positive $\Phi_+ > 0$ and negative $\Phi_- < 0$ fluxes

$$\varepsilon = \frac{2\Phi_{tot}}{(\Phi_+ + |\Phi_-|)}, \tag{13}$$

is small. A second validation of the theory is related only to the 'deviated' parts of a flux, i.e., those parts along the cross-section in which the flux Φ_{errHs} should be downwind for depths $H_s < \langle H\rangle$, but is actually upwind (it is 'wrong') and in which the flux Φ_{errHg} is downwind for depths $H_g > \langle H\rangle$ instead of being upwind (also 'wrong'). Since the southern wind opposes the vector that is normal to the cross-section of the northern Adriatic (Figure 1, full red line), while the ENE bora wind is in the direction of the normal vector of the cross-section of the Gulf (Figure 1, dashed red line), the signs of Φ_{errHs} and Φ_{errHg} are reversed in both cases (Table 1). Nonetheless, the second measure of the deviation from simplified topographic control is defined for both cross-sections (the northern Adriatic and the Gulf of Trieste) as:

$$\varepsilon_{err} = \frac{2\left(\left|\Phi_{errHg}\right| + \left|\Phi_{errHs}\right|\right)}{(\Phi_+ + |\Phi_-|)}. \tag{14}$$

4. Results

4.1. Horizontal Distribution of Wind-Driven Currents

[36] We shall first have a look at the horizontal distribution of currents at 1 m depth and 15 m depth for the situations during the southern jugo wind (28–30 October 2008; Figure 5) and during the bora ENE wind (19–21 March 2009). During the southern jugo or sirocco wind, currents near the surface and at 15 m depth are generally oriented toward north and are stronger in this direction on the eastern side of the model domain, where the southern wind is stronger (Figure 3, left). In the southern part of the model

Table 1. Fluxes and Their Errors Through the Cross-Sections (See Figure 1 for Their Locations) During the Southern Jugo Wind on 28–30 October 2008 Over the Northern Adriatic (NA) and During the ENE Bora Wind on 19–21 March 2009 Over the Gulf of Trieste (TS)[a]

Type	L (km)	$\langle H \rangle$ (m)	Φ_{tot} (10^3 m^3/s)	Φ_+ (10^3 m^3/s)	Φ_- (10^3 m^3/s)	ε (%)	Φ_{errHs} (10^3 m^3/s)	Φ_{errHg} (10^3 m^3/s)	ε_{err} (%)
Jugo/NA	123	31.9	−2.85	34.49	−37.34	7.95	2.51	−23.24	71.7
Bora/TS	21	15.4	−0.19	8.49	−8.68	2.16	0	1.52	17.8

[a]L is the cross-section length, $\langle H \rangle$ the mean depth, Φ_{tot} is the volume flux (12) through the cross-section, Φ_+ the positive part of Φ_{tot}, Φ_- its negative part, the relative ratio ε is defined in (13), Φ_{errHs} is the erroneous flux where $H_s < \langle H \rangle$ and Φ_{errHg} the erroneous flux where $H_g > \langle H \rangle$, while the second error measure ε_{err} is defined in (14).

domain they are in a NE direction toward the peninsula of Istria (see Figure 1 for geographic notations). A cyclonic turn is present in the area north of the Po River Delta (12.7–13.3°E, 45.0–45.5°N). A strong narrow coastal current in a SW direction carries the water mass from the outfall of the Tagliamento River (Figure 1) toward the outfall of the river Brenta. The northward current near the sea-surface south of the outflow of the Tagliamento splits into two parts. The part westward of the outflow of the Tagliamento (long. < 13.1°E, 45.6°N) composes the major central cyclonic turn, while its eastward part (long. > 13.1°E), turns eastward and brings the water mass into the Gulf of Trieste ('Gulf'; long. > 13.5°E, and lat. > 45.5°N) mostly at its *northern* side. Along the southern coastline of the Gulf the surface flow crosses the Gulf toward the northeastern corner inside the Gulf and does not leave it.

[37] At a depth of 15 m (Figure 5, bottom left) there is an outflow along the southern coastline of the Gulf, where the area is deeper than on the northern side of the Gulf. However, over the whole model domain at a depth of 15 m the southern wind induces cyclonic circulation in the central northern half of the model domain (12.9–13.5°E, 44.7–45.4°N), with a relatively strong current that crosses the full line in a SE direction in the central part of the profile line. In the western part of the model domain north of the Po River Delta there is a broad region of southwestward currents toward the coastline just north of this delta.

[38] When the ENE bora wind blows (Figure 5, right), the cyclonic circulation is clearer than in the case of the southern

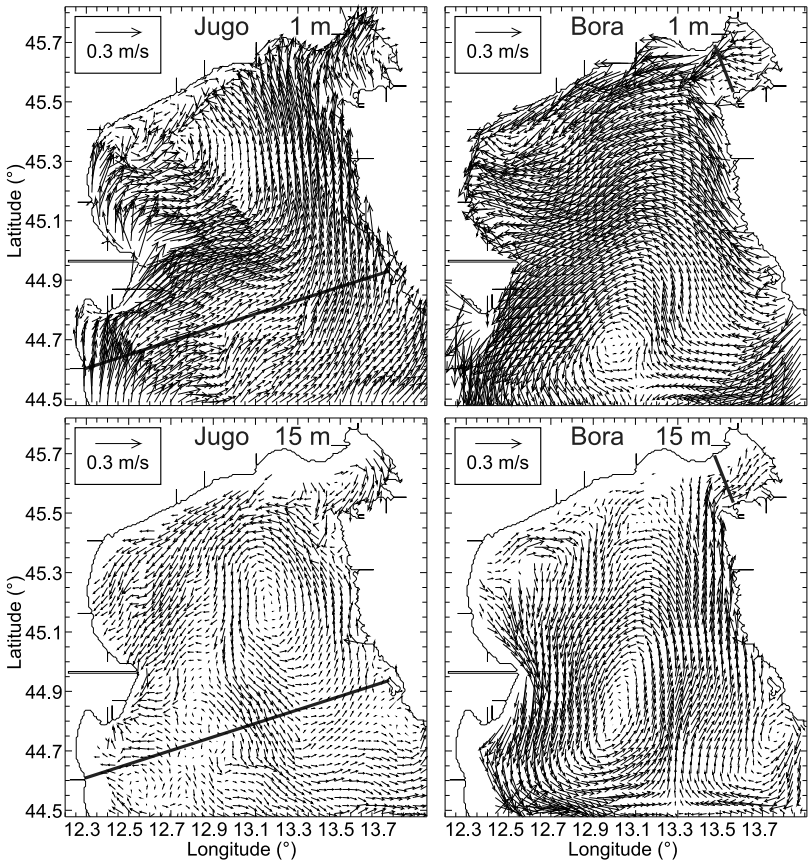

Figure 5. (left) Horizontal distribution of mean currents (top) at 1 m depth and (bottom) at 15 m depth during the southern jugo wind, where hourly values of currents were averaged in time over the interval 28–30 October 2008, and (right) the same distributions during the bora wind, where currents were averaged over the interval 19–21 March 2009. For the sake of clarity vectors in every fifth model cell are presented with a space separation ∼3.0 km.

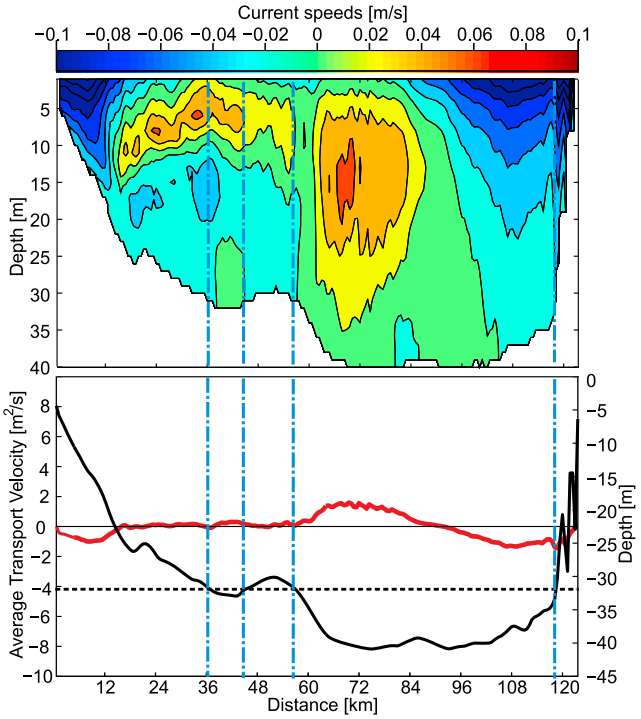

Figure 6. (top) Vertical distribution of average currents normal to the cross-section line (see Figure 5 for its position) during the southern jugo wind 28–30 October 2008. (bottom) The red line represents the transport (vertical integral of velocities from the bottom to the surface). Its axis is on the left-hand side of the plots. The black line is the bottom topography with the corresponding axis on the right-hand side of the plots. The left-hand side of the plots is near the Italian coastline, while the right-hand side is close to the Croatian coastline. Vertical dash-dotted lines mark the positions at which the depth of the seafloor meets the average cross-section depth (horizontal black dashed line) and at which the transport should change sign according to a simple theory of topographic control. Negative velocities (transports) are those that are close to the wind direction near coastlines, while positive velocities are in the direction of the vector normal to the transect line. The normal vector points out of the model domain toward the OB lines, in a direction that is nearly opposite the direction of the southern wind.

wind. It is in the form of a closed, asymmetric gyre, present near the sea-surface (Figure 5, top right) as well as at depth (Figure 5, bottom right). The gyre is elongated and rotated, the longer axis with smaller velocities is roughly along the line of minima wind speeds (Figure 3, right) that connects points (12.7°E, 44.5°N) and (13.6°E, 45.0°N) In this wind-drive, however, there is a southwestward current of this cyclonic gyre from the central northern region (12.9–13.3°E, 45.3–45.6°N) toward the Po River Delta – contrary to what was observed at the surface under jugo wind-forcing. Under the bora there is a 'diagonal' outflow, in which the water mass near the sea-surface deep inside the Gulf near the southern coastline (13.7°E, 45.55°N) crosses the Gulf diagonally and reaches the northern coastline at the northern edge of the Gulf's entrance (13.4°E, 45.65°N). This surface outflow will be further elucidated in Discussion.

[39] At 15 m depth (Figure 5, bottom right) the western part of the coastal current along the peninsula of Istria separates in a westward direction from it, while the eastern part next to the coastline turns eastward in the Gulf against the ENE wind, where the Istria peninsula ends (13.45°E, 45.5°N). This inflow coastal current in the Gulf along its southern coastline at a depth of 15 m, certainly 'holds water'. The vertical profile of ADCP velocity measurements at Vida during winter also reproduces it [*Malačič and Petelin*, 2006, 2009].

[40] We close the review of the horizontal distribution of currents during the bora in another area – south of the southern tip of the peninsula of Istria (lon. > 13.7°E, lat. < 44.75°N), by identifying a strong surface current in a southwest direction (Figure 5, top right), where the current at 15 m depth follows the direction of the surface current. This agrees with a zone of the stronger bora wind (Figure 3) in that area, which emerges from the Bay of Kvarner, not covered by the model. Along the southern OB line (lat. < 44.5°N), however, east-west currents are certainly artificial and this we could not avoid by applying several OB conditions [*Arnold*, 1987; *Blumberg and Mellor*, 1987; *Kuzmić and Orlić*, 1985].

4.2. Vertical Profiles of Wind-Driven Currents

[41] While the horizontal view of currents gave an impression regarding the distribution of gyres and currents, it is the view in a vertical plane that will complement previous pictures and will also test the validity of a simplified view of the topographic control of wind-driven circulation, adopted from a theory of elongated basins [*Csanady*, 1982].

[42] The vertical distribution of average currents and transport normal to the line, which is roughly orthogonal to the southern jugo wind on 28–30 October 2008 (Figure 3, left) is presented in Figure 6. While instantaneous (hourly) normal velocities would be modulated in a rhythm of tides, we observe on Figure 6 that normal velocities (and transports), averaged over 72 h are negative (blue areas) near the coastlines where currents flow into the model domain (nearly) parallel to the wind, away from the OB lines. Positive velocities (red areas) and transports are found in the central, deeper part and are opposite to the wind direction. Very roughly, this agrees with the statement written below (12). There is quite a large segment along the transect (18 km < distance < 57 km) where the normal transport (red line) is weak, close to zero. Along this segment, velocities in the upper part of the water column, with depths < 15 m are positive in the upwind direction out of the model domain, while those at greater depths have a normal component in the downwind direction. The simulation reproduces a thin surface layer, a few meters thick at most, in which normal currents are in the direction of the wind, which goes to zero at a point with distance = 36 km. Below it there is a layer (with depths < 15 m) of relatively strong currents opposing the wind. The transport is close to zero, although it should be much more negative in the interval 18 km < distance < 36 km. However, along the rest of the segment (36 km < distance < 57 km) the cross-section depth is close to the average depth, where weak transport is expected. Another quite large area of 'wrong' transport is closer to the right-

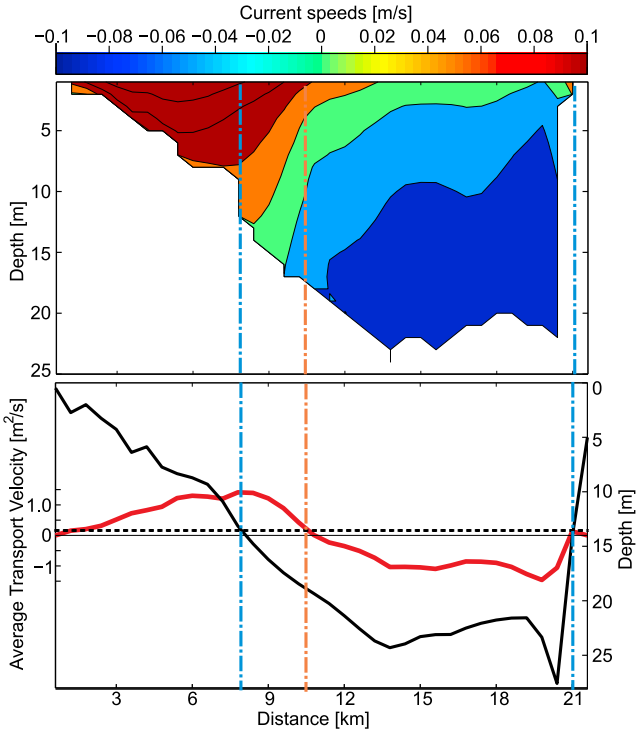

Figure 7. Same as in Figure 6, except for the cross-section line in the Gulf of Trieste which is nearly orthogonal to the bora wind that blew 19–21 March 2009 (Figure 3, right). The left side of the x axis is near the shallower northern (Italian) coastline of the Gulf, while the right side ($x > 35$) is in the vicinity of the southern (Slovenian) coastline of the Gulf. In contrast to Figure 6, negative average velocities (transports) are almost all found in the central, deeper part of the transect and are (nearly) opposite to the direction of the ENE wind. Positive velocities are near the coastlines, they are in the direction of a normal vector that points out of the Gulf, and are nearly parallel to the wind.

hand side of plots, for the segment 93 km < distance < 120 km. There the transport is negative, while it should be positive (upwind), because the depth is greater than the average depth. However, the area with the wind-driven current extends offshore from the coastline (distance > 120 km) in the transect interior, toward a distance = 90 km. Quantitative evaluation of the transport with the simplified theory will follow in Table 1.

[43] When the bora wind was blowing (Figure 7), the transport and normal velocities were observed along a much shorter cross-section (distance 21 km) than that across the northern Adriatic in the case of the southern wind (distance = 123 km). This time, model results look much better when compared to a simplified analytical model of topographic control by (12). Near the northern (Italian) coastline (distance near zero) we observe positive currents (Figure 7, top) and transports (Figure 7 (bottom), red line), now nearly aligned with the ENE bora wind. At the other side of the transect (distance = 21 km), near the southern (Slovenian) coastline we observe a very small area of positive normal velocity aligned with the wind, with slightly positive values of a transport. A closer look at the distribution of normal velocities shows that the transport changes sign at a distance = 10 km, while measurements indicate the change to be at 8 km distance, where the depth equals the cross-section average.

[44] Quantitative deviation from the topographic control, tested with NAPOM, is summarized in Table 1. We observe that in both wind-driven cases, jugo, as well as bora, the relative error of the flux, defined by (13) is low enough ($\varepsilon <$ 8% under jugo forcing over the northern Adriatic and $\varepsilon <$ 2.2% under bora forcing over the Gulf of Trieste). It is reasonable that for jugo driven circulation ε is larger – the model domain is relatively wide and large and the water mass could enter more than exit ($|\Phi_-| > \Phi_+$) over a three day interval. The inflow matches the outflow quite well for the smaller Gulf of Trieste during the bora over a three day period. However, the match of the flow which should be downwind in shallow areas and upwind in deeper areas quantitatively fails for the cross-section through the northern Adriatic ($\varepsilon_{err} < 72\%$) during the jugo wind. Obviously, large flow rates are present in a 'wrong direction'. The relatively solid match ($\varepsilon_{err} < 18\%$) of NAPOM with the simple theory of topographic control in an elongated basin is found for the flow rate through the cross-section in the Gulf of Trieste during the bora.

4.3. ALADIN/SI Winds and NAPOM Currents

[45] The vertical distribution of measured currents and NAPOM results at the location of the coastal buoy Vida (Figure 1 for the location) are presented in Figure 8. For clarity only the component normal to the cross-section line in the Gulf is presented. The vertical distribution of currents clearly stands out from measurements (red line). The simulation (black line) shows some variation of currents along the vertical in the upper half of the water column and within its bottom 6–7 m. The latter variation is due to friction near the seafloor. In the top part of the water column it smoothly follows the vertical distribution of measured currents, although the sign near the sea-surface is wrong in the jugo wind-driven situation (left). In the bora wind-driven situation (right) we observe in simulations the same sign of the normal component of currents near the sea-surface as in measurements (red).

[46] Before entering into a quantitative skill assessment of NAPOM results at Vida, we have to be clear about the meteorological ALADIN/SI forecast at that location. Table 2 depicts the statistics regarding the efficiency of ALADIN/SI and we observe that the absolute mean bias (*MB*) of each component is below 2.4 m/s, the largest being for the northern (smaller) component during the ENE bora wind. The cross-correlation coefficient, and indicator of a linear relationship between the model and measurements, is relatively low ($0.5 < CC < 0.6$) for the southern jugo wind, while it is better for the bora wind ($0.7 < CC < 0.9$). The mean square error (*MSE*), which is the last 'measure' of model agreement with measurements for winds, is quite high for the eastern component during the jugo ($MSE > 18$ m^2/s^2), but is lower for the northern component ($MSE < 11$ m^2/s^2) during the jugo, which is lower than components during the bora wind (13.5 m^2/s^2 < *MSE* < 13.9 m^2/s^2). This sounds important since it is the northern component during the jugo that dominates ($\bar{o} = 7.94$ m/s). However, the sum of *MSE* of both components is also indicative of wind as a vector. *MSE* equals 29.1 m^2/s^2 and 27.4 m^2/s^2 for the southern and the

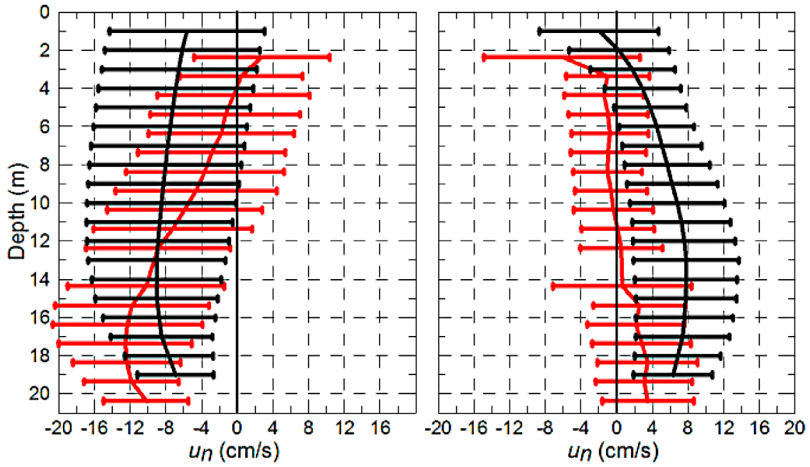

Figure 8. Vertical distribution of the mean currents over 72 h at buoy Vida (left) during the southern jugo wind on 28–30 October 2008 and (right) during the ENE bora wind on 19–21 March 2009. Only currents normal to the cross-section line of the Gulf of Trieste are presented (see Figure 1 for the location of the buoy Vida and the red dashed line of the cross-section). Red: ADCP measurements at 17 depths, black: NAPOM simulations. Horizontal bars represent two standard deviations of currents around the mean.

ENE winds, respectively. These values are quite close. We cannot definitively conclude that the ALADIN/SI model gave better results during the jugo or during the bora. Of the two particular three-day windy situations studied here, simulations were slightly better during the bora wind from the point of *CC* and *MSE*.

[47] In the assessment of NAPOM with measured currents at the location of the coastal buoy Vida we observe in Table 3 that the mean bias is larger for the normal (orthogonal to the cross-section in the Gulf) component of currents during the bora (=5.5 cm/s). Measurements show that the mean current in time and along the water column is close to zero (0.12 cm/s), which is not reproduced by NAPOM. Under the jugo wind the $MB < 2.3$ cm/s.

5. Discussion

[48] We will present mechanisms that affect numerical model results, especially those that seem to be linked to wind-driven transport and were not captured with a simple analytical model of topographic control.

[49] In the applied boundary condition for turbulence production at the surface (1) the turbulence production due to the breaking of surface waves is not excluded, but this effect should be better accounted for with parameterization (3). However, simulations with the latter clearly showed that in the case of parameterization the vertical profile of mean currents at the position of the coastal buoy is too homogenized in both wind-driven situations and was therefore not chosen for further simulations. These simulations had an insignificant effect on the transport through the observed transects and were therefore not presented. The match of model results during the bora episode with simple analytical reasoning of topographic control along the entrance to the Gulf holds firm, despite the significant upward surface heat flux during the bora [*Dorman et al.*, 2007], which was ignored in the simplified approach and the topographic control of bora driven circulation was therefore surprising. As is shown here, forced mixing and convective overturns seem not to seriously affect the topographic control of wind-driven circulation when the stratification is weak, at least during the bora wind in the Gulf of Trieste. The second reason why topographic control of the wind-driven circulation in the Gulf of Trieste during the bora was not expected is the complexity of circulation over the northern Adriatic, related to the distribution of a wind stress torque, observed from different aspects by many previous studies [*Bignami et al.*, 2007; *Kuzmić et al.*, 2006; *Lee et al.*, 2005; *Martin et al.*, 2006; *Orlić et al.*, 1986, 1994; *Pullen et al.*, 2003; *Zore-Armanda and Gačić*, 1987]. A reproduction with NAPOM was made of a known double gyre circulation due to the bora wind vorticity, which results from a stronger wind over the Gulf, a strong wind south of the peninsula of Istria and a weaker wind in between, resulting in a cyclonic circulation between the north side of the Istria peninsula and the Italian coastline north of Po River Delta,

Table 2. Statistical Comparison of ALADIN/SI Forecast and Measurements (Hourly Values) During the Southern Jugo Wind on 28–30 October 2008 and During the ENE Bora Wind on 19–21 March 2009 at the Position of Buoy Vida[a]

Type	Component	$\bar{m}$ (m/s)	$\bar{o}$ (m/s)	*MB* (m/s)	S_m (m/s)	S_o (m/s)	*SDE* (m/s)	*CC* (1)	*MSE* (m^2/s^2)
Jugo/Vida	East	−0.64	0.76	−1.40	3.59	4.62	−1.03	0.54	18.12
	North	8.93	7.94	0.99	2.16	3.91	−1.75	0.59	10.98
Bora/Vida	East	−5.98	−7.99	1.99	3.43	5.74	−2.31	0.89	13.87
	North	−4.11	−1.73	−2.38	3.90	3.67	0.23	0.73	13.53

[a]The amount of the data $N = 72$. See the text in section 2.4 and the expression (5) for the meaning of column labels. The mean observed wind speed in both situations was over 8 m/s.

Table 3. Statistics of the NAPOM Skill When Compared With ADCP Measurements of Currents (Hourly Values) During the Southern Jugo Wind on 28–30 October 2008 and During the ENE Bora Wind on 19–21 March 2009 at the Position of Buoy Vida (Figure 1 for the Location)[a]

Type	Component	$\bar{m}$ (cm/s)	$\bar{o}$ (cm/s)	*MB* (cm/s)	S_m (cm/s)	S_o (cm/s)	*SDE* (cm/s)	*CC* (1)	*MSE* (cm^2/s^2)
Jugo	normal	−7.91	−6.16	−1.75	7.67	9.42	−1.75	0.68	52.77
	tangential	−0.75	1.52	−2.27	4.71	7.06	−2.35	0.46	46.69
Bora	normal	5.62	0.12	5.50	5.45	5.69	−0.24	0.64	52.84
	tangential	−0.22	0.21	−0.43	2.78	4.37	−1.59	0.27	20.48

[a]See section 2.4 and expression (5) for the meaning of quantities. Model currents at similar depths (e.g., 2 m, 3 m, …, 19 m) were compared to measured currents (mean depths 2.355 m, 3.355 m, …19.355 m). The amount of the data N = 1224 (=72*17).

and the anticyclonic (not closed) circulation between the Italian coastline south of the delta and the peninsula of Istria. With NAPOM we did not directly reproduce the transport of a surface fresher water mass, which emerges from the Po River Delta and acts as a passive tracer toward the Gulf of Trieste as an oblique current during the winter bora event [*Cushman-Roisin and Korotenko*, 2007; *Kuzmić et al.*, 2006]. This, however, also depends strongly upon the details of the distribution of the wind stress in a particular synoptic situation. The bora wind in Figure 3 is close to the RADARSAT distribution of the bora wind [*Lee et al.*, 2005, Figure 1b] on another occasion (12th February 2003); in both cases there is a weak bora in front of the middle part of the peninsula of Istria, which spreads in a SW direction.

[50] The reasoning that the bora wind may not always drive the oblique surface current of fresh water from the Po River to the Gulf was also confirmed in one of the latest studies [*Boldrin et al.*, 2009], in which it is clearly shown that the diagonal area of wind minima, when the two bora jets are present, is several tens of km southward of the entrance to the Gulf (see the wind stress on 26 September 2002 shown by *Boldrin et al.* [2009, Figure 3]).

[51] The model failed to quantitatively reproduce simple topographic control when the southern wind blows over the northern Adriatic. This, however, does not mean that the bottom topography is irrelevant and it should be explored in the future with a more elaborated concept. The topography also changes *along* the elongated basin (Adriatic), not only across it, which was not considered in our study. However, through the Gulf of Trieste the circulation is simpler during the bora; it is dominated by topographic control, for up to 100% − ε_{err} = 82.2% of the flux (see Table 1 for ε_{err}). Moreover, we should not ignore the importance of horizontal wind shear. The jugo wind increases in intensity from the western to the eastern coastline (Figure 3), which is not embraced in a simplified theory of topographic control.

[52] Numerical simulations of the spread of turbid Po River waters using the ROMS model and the LAMI wind field are presented in *Bignami et al.* [2007]. In the northern Adriatic they obtained the eastward across-basin currents at the southern edge of the NAPOM model domain, which agrees with the results presented here in Figure 5. In the bora wind-driven situation [*Bignami et al.*, 2007] they also obtained major features of surface circulation [*Bignami et al.*, 2007, Figure 8] over the northern Adriatic that were here presented. Recent [*Russo et al.*, 2009] and ongoing [*Russo et al.*, 2012] operational efforts in the Adriatic, that include wave-current interactions, express these circulation features in more detail.

[53] The simulation pictures a diagonal crossing of the Gulf of Trieste at the sea-surface (Figure 5, top right), leading the water mass in a NW direction from the southern inside part of the Gulf to the northern coastline at the Gulf's entrance. This was observed numerically in a climatic circulation of the Gulf during winter [*Malačič and Petelin*, 2009], when the bora wind dominates. This surface circulation, however, was also reproduced by a synoptic circulation model of completely different architecture, with which the unsteady synoptic bora-driven circulation in the Gulf during summer was studied [*Querin et al.*, 2007]. Numerical simulations with a third type of model architecture (Mike 3 and PCFLOW3D) [*Dorić*, 2008], also demonstrate a very similar deviation of the surface current to the right from the wind direction during the bora episode, which agrees with one of the first simulations of the synoptic circulations of the Gulf [*Rajar*, 1989].

[54] These model results should be explored in the future in a more careful way in light of a recent analytical study of coastal upwelling using a linear reduced gravity model, in which the wind stress oscillates and may also rotate [*Orlić and Pasarić*, 2011]. It was found that in the upper layer (the 'deep' bottom layer is still) the alongshore wind mostly contributes to sub-inertial variability with the exponential offshore trend scaled as $R_a = (g'h/(f^2 - \omega^2))^{1/2}$ (g' is the reduced gravity = $g\varepsilon$, h the mean thickness of the upper layer), which converges to the Ekman type of motion when $\omega \to 0$. A linear theory from a reduced gravity model is of doubtful use due to the large vertical motions of the pycnocline under weak stratification and strong winds, as it is in the examples explored here.

[55] Inertial motion has many different aspects that are certainly not covered by this paper, e.g., the oscillation of a pycnocline [*Krajcar and Orlić*, 1995; *Orlić*, 1987] and the erosion of the pycnocline, mostly during the first inertial period [*Pollard et al.*, 1972]. Additional comment related to inertial oscillations also seems appropriate. Although by averaging operational model results (currents) over a sufficiently long period (72 h) one retrieves the net-transport over the averaging period, this does not mean that the 'disturbing' periodic motion, e.g., tides, and inertial motion in particular, have been effectively removed. A better way would be the narrow band filtering of currents around the inertial period and (seven) tidal periods. This, however, means a much longer time series (months) rather than just a few days, obtained by simulations under a long-lasting artificial steady wind. Since tidal currents hardly surpass 0.05 m/s, they do not contribute significantly (through residual tides) to transport over larger distances and residuals are limited to

areas around promontories and river outlets [*Cushman-Roisin and Naimie*, 2002; *Malačič and Viezzoli*, 2000].

[56] The rotation of the Earth modifies the along basin motion in relatively narrow channels [*Gill*, 1979]. We may apply similar reasoning to wind-driven transport analysis, where the Coriolis effect will be treated as a correction to the non-rotated basin, where only the transport along the basin and the sea-surface elevation are considered. In the cross-basin equation of motion, the second expression in (8), which has not yet been considered, we supposed that $V \ll U$ and therefore $\partial\eta/\partial y \cong 0$. The Coriolis term changes the balance into:

$$\frac{\partial V}{\partial t} + fU = -gH\frac{\partial \eta}{\partial y} \tag{15}$$

in which still $V \ll U$, or better $\Delta V/U \ll (f\Delta t) < 1$, where the time scale of local acceleration Δt is still shorter than $2\pi/f$, which is required for the approximation (8) of the equation of motion along the basin. This leads to a geostrophic approximation in a cross-basin direction, which could be integrated over it:

$$\eta_R = \eta - \frac{f\,L\langle U\rangle}{gH}, \tag{16}$$

where $\langle U\rangle$ is the along basin transport, averaged over its width L and η_R the elevation which is corrected by the Coriolis term with respect to η without it. The expression (16) seems to contradict (9), which lead to (12) together with the hypothesis of zero flux through the cross-section: $L\langle U\rangle = 0$. However, (16) means the correction in η due to the Earth's rotation 'violates' the condition $L\langle U\rangle = 0$ on a non-rotating elongated basin and we also have to look at it from the standpoint of long traveling (Kelvin) waves which may travel with tidal periods along the basin. It can easily be shown from the equations for traveling non-dispersive disturbances with a speed $c = (gH)^{0.5}$ that the transport amplitude $\langle U\rangle_0 = (gH)^{0.5}\,Z_0$, where Z_0 is the amplitude of η. The amplitude of the correction term for η_R in (16) due to rotation of the basin, relative to Z_0, therefore equals to L/R, with the barotropic Rossby radius of deformation $R = (gH)^{0.5}/f$. For the line between the Italian and Croatian coasts see (Figure 1, full red line) $L = 120$ km. Modeled depths along that profile vary around the mean value $\langle H\rangle = 32$ m with SD = 9 m, both are close to the mean and standard deviation of the whole model area ($\langle H\rangle = 30$ m with SD = 11 m). The first quartile of depths is reached for $0 \le H \le 28$ m, the median value is 33 m (of the whole model area 31 m) and the third quartile of depths is reached at 40 m. This leads to 166 km $\le R \le$ 188 km and $0.6 \le L/R \le 0.8$, if we consider for R the depths of the first and of the third quartile. A slightly narrower interval would be obtained if the mean value and the SD would be applied ($\langle H\rangle$ − SD and $\langle H\rangle$ + SD) in the estimate of variations of L/R across the northern Adriatic. Over all, it is obvious that the 'correction' term is important: values of L/R close to 1 (wide channel) indicate that the across-channel velocity component is certainly not negligible, nor are other long waves (e.g., the Poincaré waves), in addition to the Kelvin waves.

[57] A similar estimate for the cross-section of the Gulf (Figure 1, dashed red line) can be made, for which L = 20 km, $\langle H\rangle = 15$ m, SD = 8 m, 1st quartile is reached for depths around 8 m, the 3rd quartile at depth 22.5 m, median is 18 m, leading to 90 km $\le R \le$ 150 km and $0.1 \le L/R < 0.3$. This still means that the correction term in (16) is justified, being 'small enough'.

6. Conclusions

[58] In this study we have verified with a model a simple theory of the topographic control of the two most-frequent Adriatic wind-driven circulations. The model fairly reproduced key circulation patterns during the ENE bora wind (e.g., the northern cyclonic gyre, from which a smaller branch separates at the northern end of peninsula of Istria which brings the water mass at depth into the Gulf of Trieste along its southern coastline, and, at the surface, the diagonal outflow from the Gulf of Trieste). The model also clearly showed the wind-driven structure of circulation during the southern wind, the cyclonic turn in the central part of the northern Adriatic and the split off current in front of the northern coastline of the entrance to the Gulf of Trieste. We demonstrated that the hypothesis of a zero flux through the vertical cross-section of the northern Adriatic during a southern wind holds for 92% of the flow. We also showed that almost complete agreement (98%) with the zero flux hypothesis is achieved for a flux through a transect at the entrance to the Gulf of Trieste during the bora wind. During the southern wind the simple theory of a topographic control over the relatively wide northern Adriatic quantitatively fails. The theory still holds qualitatively over the shallow banks near the coastlines, where the mean transport is downwind, and also in deeper parts, where the transport is upwind. However, the dominant topographic control is quantitatively confirmed during the bora wind for the transport of water mass at the entrance to the Gulf of Trieste: over 82% of the flux follows topographic control.

[59] Model results were also validated with measurements at a coastal buoy at the entrance to the Gulf of Trieste. The cross-correlation of model values with measurements are CC = 0.68 for the dominant component normal to the cross-section of the Gulf during the jugo wind and CC = 0.64 during the bora wind. In addition, the atmospheric Aladin/SI model hindcast winds during the southern wind had a relatively modest agreement with buoy Vida measurements (CC = 0.59), while model winds reached a strong agreement with measurements (CC = 0.89) during the bora wind.

[60] **Acknowledgments.** This research is part of a research program funded by the Ministry of Higher Education and Technology of Slovenia (contract P1-0237) and is also funded by the EC project 'MyOcean', grant agreement 218812.

References

Accerboni, E., F. Castelli, and F. Mosetti (1971), Sull'uso dei modelli matematici idrodinamici per lo studio dell'acqua alta a Venezia, *Boll. Geofis. Teor. Appl.*, *13*(49), 18–35.

Arnold, R. J. (1987), In improved open boundary condition for a tidal model of Bass Strait, in *Numerical Modelling: Applications to Marine Systems*, edited by J. Noye, pp. 145–158, Elsevier, Amsterdam, doi:10.1016/S0304-0208(08)70033-1.

Bénard, P., J. Vivoda, J. Mašek, P. Smolikova, K. Yessad, C. Smith, R. Brožkova, and J.-F. Geleyn (2010), Dynamical kernel of the Aladin-NH spectral limited-area model: Revised formulation and sensitivity experiments, *Q. J. R. Meteorol. Soc.*, *136*, 155–169, doi:10.1002/qj.522.

Bignami, F., R. Sciarra, S. Carniel, and R. Santoleri (2007), Variability of Adriatic Sea coastal turbid waters from SeaWiFS imagery, *J. Geophys. Res.*, *112*, C03S10, doi:10.1029/2006JC003518.

Blumberg, A. F., and G. L. Mellor (1987), A description of a three-dimensional coastal ocean circulation model, in *Three-Dimensional Coastal Ocean Models*, *Coastal Estuarine Sci.*, vol. 4, edited by N. S. Heaps, pp. 1–16, AGU, Washington, D. C., doi:10.1029/CO004p0001.

Boldrin, A., S. Carniel, M. Giani, M. Marini, F. Bernardi Aubry, A. Campanelli, F. Grilli, and A. Russo (2009), Effects of bora wind on physical and biogeochemical properties of stratified waters in the northern Adriatic, *J. Geophys. Res.*, *114*, C08S92, doi:10.1029/2008JC004837.

Carniel, S., J. C. Warner, J. Chiggiato, and M. Sclavo (2009), Investigating the impact of surface wave breaking on modeling the trajectories of drifters in the northern Adriatic Sea during a wind-storm event, *Ocean Modell.*, *30*(2–3), 225–239, doi:10.1016/j.ocemod.2009.07.001.

Charnock, H. (1955), Wind stress on a water surface, *Q. J. R. Meteorol. Soc.*, *81*, 639–640, doi:10.1002/qj.49708135027.

Chiggiato, J., and P. Oddo (2008), Operational ocean models in the Adriatic Sea: A skill assessment, *Ocean Sci.*, *4*, 61–71, doi:10.5194/os-4-61-2008.

Craig, P. D., and M. L. Banner (1994), Modeling wave-enhanced turbulence in the ocean surface layer, *J. Phys. Oceanogr.*, *24*(12), 2546–2559, doi:10.1175/1520-0485(1994)024<2546:MWETIT>2.0.CO;2.

Csanady, G. T. (1982), *Circulation in the Coastal Ocean*, 279 pp., D. Reidel, Dordrecht, Netherlands.

Cushman-Roisin, B., and K. A. Korotenko (2007), Mesoscale-resolving simulations of summer and winter bora events in the Adriatic Sea, *J. Geophys. Res.*, *112*, C11S91, doi:10.1029/2006JC003516.

Cushman-Roisin, B., and C. E. Naimie (2002), A 3D finite-element model of the Adriatic tides, *J. Mar. Syst.*, *37*, 279–297, doi:10.1016/S0924-7963(02)00204-X.

Cushman-Roisin, B., V. Malačič, and M. Gačić (2001), Tides, seiches and low-frequency oscillations, in *Physical Oceanography of the Adriatic Sea, Past, Present and Future*, edited by B. Cushman-Roisin et al., pp. 217–240, Kluwer Acad., Dordrecht, Netherlands.

Dorić, E. (2008), A comparison of the MIKE 3 and PCFLOW3D models for hydrodynamic simulations in the Gulf of Trieste [in Slovenian], B. Sci. thesis, Fac. of Civ. Eng. and Geod. Univ. of Ljubljana, Ljublana.

Dorman, C., et al. (2007), February 2003 marine atmospheric conditions and the bora over the northern Adriatic, *J. Geophys. Res.*, *111*, C03S03, doi:10.1029/2005JC003134. [Printed *112*(C3), 2007.]

Flather, R. A. (1976), A tidal model of the north-west European Continental Shelf, *Mem. Soc. R. Sci. Liege*, *6*(10), 141–164.

Gill, A. (1979), *Atmosphere-Ocean Dynamics*, 662 pp., Academic, London.

Heaps, N. S. (1972), On the numerical solution of the three-dimensional hydrodynamical equations for tides and storm surges, in *Third Liège Colloquium on Ocean Hydrodynamics*, edited by J. J. Nihoul, pp. 143–180, Univ. of Liège, Liège, Belgium.

Hendershott, M. C., and P. Rizzoli (1976), The winter circulation of the Adriatic, *Deep Sea Res.*, *23*, 353–370.

Huang, C. J., F. Qiao, Z. Song, and T. Ezer (2011), Improving simulations of the upper ocean by inclusion of surface waves in the Mellor-Yamada turbulence scheme, *J. Geophys. Res.*, *116*, C01007, doi:10.1029/2010JC006320.

Janeković, I., and M. Kuzmić (2005), Numerical simulation of the Adriatic Sea principal tidal constituents, *Ann. Geophys.*, *23*, 3207–3218, doi:10.5194/angeo-23-3207-2005.

Jeffries, M. A., and C. M. Lee (2007), A climatology of the northern Adriatic Sea's response to bora and river forcing, *J. Geophys. Res.*, *112*, C03S02, doi:10.1029/2006JC003664.

Jeromel, M., V. Malačič, and J. Rakovec (2009), Weibull distribution of bora and sirocco winds in the northern Adriatic Sea, *Geofizika*, *26*(1), 85–100.

Killworth, P. D. (1996), Time interpolation of forcing fields in ocean models, *J. Phys. Oceanogr.*, *26*, 136–143, doi:10.1175/1520-0485(1996)026<0136:TIOFFI>2.0.CO;2.

Krajcar, V., and M. Orlić (1995), Seasonal variability of inertial oscillations in the Northern Adriatic, *Cont. Shelf Res.*, *15*(10), 1221–1233, doi:10.1016/0278-4343(94)00077-Z.

Kuzmić, M., and M. Orlić (1985), A study of the influence of open-boundary conditions on the predictions of a wind-driven model, *Rapp. Comm. Int. Mer Méditerr.*, *29*, pp. 75–78, Comm. Sci. de la Méditerr., Monaco.

Kuzmić, M., M. Orlić, M. Karabeg, and L. Jeftić (1985), An investigation of wind-driven topographically controlled motions in the northern Adriatic, *Estuarine Coastal Shelf Sci.*, *21*, 481–499, doi:10.1016/0272-7714(85)90052-6.

Kuzmić, M., I. Janeković, J. W. Book, P. J. Martin, and J. D. Doyle (2006), Modeling the northern Adriatic double-gyre response to intense bora wind: A revisit, *J. Geophys. Res.*, *111*, C03S13, doi:10.1029/2005JC003377. [Printed *112*(C3), 2007.]

LeBlond, P. H., and L. A. Mysak (1988), *Waves in the Ocean*, 602 pp., Elsevier, Amsterdam.

Lee, C. M., et al. (2005), Northern Adriatic response to a wintertime bora wind event, *Eos Trans. AGU*, *86*(16), 157.

Malačič, V., and B. Petelin (2004), MFSTEP—Mediterranean ocean Forecasting System: Toward environmental predictions (first scientific report: 1st March, 2003–29th February, 2004), inclusion of tidal and atmospheric pressure forcing, *Rep. COBISS.SI-ID 1378895*, 5 pp., Mar. Biol. Stn., Natl. Inst. of Biol., Piran, Slovenia.

Malačič, V., and B. Petelin (2006), Numerical modeling of the winter circulation of the Gulf of Trieste (northern Adriatic), *Acta Adriat.*, *47*, suppl., 207–217.

Malačič, V., and B. Petelin (2009), Climatic circulation in the Gulf of Trieste (northern Adriatic), *J. Geophys. Res.*, *114*, C07002, doi:10.1029/2008JC004904.

Malačič, V., and D. Viezzoli (2000), Tides in the northern Adriatic Sea—The Gulf of Trieste, *Nuovo Cimento Soc. Ital. Fis. C*, *23*(C4), 365–382.

Malačič, V., D. Viezzoli, and B. Cushman-Roisin (2000), Tidal dynamics in the northern Adriatic Sea, *J. Geophys. Res.*, *105*(C), 26,265–26,280.

Marsaleix, P., C. Estournel, V. Kondrachoff, and R. Vehil (1998), A numerical study of the formation of the Rhône River plume, *J. Mar. Syst.*, *14*, 99–115, doi:10.1016/S0924-7963(97)00011-0.

Martin, P. J., J. W. Book, and J. D. Doyle (2006), Simulation of the northern Adriatic circulation during winter 2003, *J. Geophys. Res.*, *111*, C03S12, doi:10.1029/2006JC003511. [Printed *112*(C3), 2007.]

Mellor, G. L. (2004), Users guide for a three-dimensional, primitive equation, numerical ocean model (June 2003 version), 53 pp., Princeton Univ., Princeton, N. J.

Mellor, G., and A. Blumberg (2004), Wave breaking and ocean surface layer thermal response, *J. Phys. Oceanogr.*, *34*(3), 693–698, doi:10.1175/2517.1.

Mellor, G. L., and T. Yamada (1982), Development of turbulence closure model for geophysical fluid problems, *Rev. Geophys.*, *20*, 851–875, doi:10.1029/RG020i004p00851.

Oddo, P., N. Pinardi, M. Zavatarelli, and A. Coluccelli (2006), The Adriatic basin forecasting system, *Acta Adriatica*, *47*, suppl., 169–184.

Oke, P. R., J. S. Allen, R. N. Miller, G. D. Egbert, J. A. Austin, J. A. Barth, T. J. Boyd, P. M. Kosro, and M. D. Levine (2002), A modeling study of the three-dimensional continental shelf circulation off Oregon. Part I: Model–data comparisons, *J. Phys. Oceanogr.*, *32*(5), 1360–1382, doi:10.1175/1520-0485(2002)032<1360:AMSOTT>2.0.CO;2.

Orlić, M. (1987), Oscillations of the inertia period on the Adriatic Sea shelf, *Cont. Shelf Res.*, *7*(6), 577–598, doi:10.1016/0278-4343(87)90024-0.

Orlić, M., and Z. Pasarić (2011), A simple analytical model of periodic coastal upwelling, *J. Phys. Oceanogr.*, *41*(6), 1271–1276, doi:10.1175/JPO-D-10-05000.1.

Orlić, M., M. Kuzmić, and Z. Vučak (1986), Wind-curl currents in the northern Adriatic and formulation of bottom friction, *Oceanol. Acta*, *9*(4), 425–431.

Orlić, M., M. Kuzmić, and Z. Pasarić (1994), Response of the Adriatic Sea to the bora and sirocco forcing, *Cont. Shelf Res.*, *14*(1), 91–116, doi:10.1016/0278-4343(94)90007-8.

Paklar, G. B., V. Isakov, D. Koračin, V. Kourafalou, and M. Orlić (2001), A case study of bora-driven flow and density changes on the Adriatic shelf (January 1987), *Cont. Shelf Res.*, *21*, 1751–1783, doi:10.1016/S0278-4343(01)00029-2.

Pollard, R. T., P. B. Rhines, and W. Thompson (1972), The deepening of the wind-mixed layer, *Geophys. Fluid Dyn.*, *4*(1), 381–404, doi:10.1080/03091927208236105.

Polli, S. (1959), La Propagazione delle Maree nell'Adriatico, paper presented at IX Convegno Dell'Associazione Geofisica Italiana, Assoc. Geofis. Ital., Rome.

Poulain, P.-M., and B. Cushman-Roisin (2001), Circulation, in *Physical Oceanography of the Adriatic Sea, Past, Present and Future*, edited by B. Cushman-Roisin et al., pp. 67–109, Kluwer Acad., Dordrecht, Netherlands.

Poulain, P.-M., V. Kourafalou, and B. Cushman-Roisin (2001), Northern Adriatic Sea, in *Physical Oceanography of the Adriatic Sea, Past, Present and Future*, edited by B. Cushman-Roisin et al., pp. 143–165, Kluwer Acad., Dordrecht, Netherlands.

Pristov, N., J. Cedilnik, B. Strajnar, J. Jerman, M. Štrajhar, and B. Muri (2011), ALADIN related activities in SLOVENIA-2011, paper presented at 21st ALADIN Workshop and HIRLAM All Staff Meeting, Swed. Meteorol. and Hydrol. Inst., Norrkoping, Sweden, 5–8 April.

Pullen, J., J. D. Doyle, R. Hodur, A. Ogston, J. W. Book, H. Perkins, and R. Signell (2003), Coupled ocean-atmosphere nested modeling of the Adriatic Sea during winter and spring 2001, *J. Geophys. Res.*, *108*(C10), 3320, doi:10.1029/2003JC001780.

Querin, S., A. Crise, D. Deponte, and C. Solidoro (2007), Numerical study of the role of wind forcing and freshwater buoyancy input on the circulation in a shallow embayment (Gulf of Trieste, Northern Adriatic Sea), *J. Geophys. Res.*, *111*, C03S16, doi:10.1029/2006JC003611. [Printed *112*(C3), 2007.]

Raicich, F. (1994), Note on the flow rates of the Adriatic rivers, *Tech. Rep., RF 02/94*, 8 pp., Ist. Sper. Talassogr., Cons. Naz. delle Ric., Trieste, Italy.

Rajar, R. (1989), Three dimensional modelling of currents in the northern Adriatic Sea, paper presented at 23rd Congress, Int. Assoc. for Hydraul. Res., Ottawa, Ont., Canada.

Rizzoli, P. M., and A. Bergamasco (1983), The dynamics of the coastal region of the northern Adriatic Sea, *J. Phys. Oceanogr.*, *13*(7), 1105–1130, doi:10.1175/1520-0485(1983)013<1105:TDOTCR>2.0.CO;2.

Robinson, A. R., A. Tomasin, and A. Artegiani (1973), Flooding of Venice: Phenomenology and prediction of the Adriatic storm surge, *Q. J. R. Meteorol. Soc.*, *99*(422), 688–692, doi:10.1002/qj.49709942210.

Russo, A., et al. (2009), An operational system for forecasting hypoxic events in the northern Adriatic Sea, *Geofizika*, *26*(2), 191–213.

Russo, A., A. Coluccelli, A. Valentini, M. Deserti, A. Benetazzo, and S. Carniel (2012), An operational coupled wave-current forecasting system for the northern Adriatic Sea, paper presented at General Assembly, Eur. Geosci. Union, Vienna.

Stacey, M. W. (1999), Simulation of the wind-forced near-surface circulation in Knight Inlet: A parameterization of the roughness length, *J. Phys. Oceanogr.*, *29*(6), 1363–1367, doi:10.1175/1520-0485(1999)029<1363:SOTWFN>2.0.CO;2.

Stravisi, F. (1972), A numerical experiment on wind effects in the Adriatic Sea, in *Atti della Accademia Nazionale dei Lincei, Estratto dai Rendiconti della Classe di Scienze fisiche, mathematiche e naturali*, pp. 187–196, Accad. Naz. dei Lincei, Rome.

Stravisi, F. (1973), Analysis of a storm surge in the Adriatic Sea by means of a two-dimensional linear model, in *Atti della Accademia Nazionale dei Lincei, Estratto dai Rendiconti della Classe di Scienze fisiche, mathematiche e naturali*, pp. 243–260, Accad. Naz. dei Lincei, Rome.

Stravisi, F. (1977), Bora driven circulation in northern Adriatic, *Boll. Geofis.*, *20*(73–74), 95–102.

World Meteorological Organization (1983), Guide to meteorological instruments and methods of observation, 5th ed., *Rep. 6.7-6*, 8 pp., Geneva, Switzerland.

Zore-Armanda, M., and M. Gačić (1987), Effects of bura on the circulation in the North Adriatic, *Ann. Geophys.*, *5B*(1), 93–102.